

Modeling solute-grain boundary interactions in a bcc Ti-Mo alloy using density functional theory

Hariharan Umashankar^a, Daniel Scheiber^b, Vsevolod I. Razumovskiy^b, Matthias Militzer^a

^a*Centre for Metallurgical Process Engineering,*

The University of British Columbia, Vancouver, BC V6T 1Z4 Canada

^b*Materials Center Leoben Forschung GmbH, Roseggerstrasse 12, Leoben 8700, Austria*

(Dated: March 6, 2025)

Solute segregation in alloys is a key phenomenon which affects various material characteristics such as embrittlement, grain growth and precipitation kinetics. In this work, the segregation energies of Y, Zr, and Nb to a $\Sigma 5$ grain boundary in a bcc Ti-25 at % Mo alloy were determined using density functional theory (DFT) calculations. A systematic approach was laid out by computing the solution energy distributions in the bulk alloy using Warren-Cowley short-range order parameters to find a representative bulk-solute reference energy. Additionally, different scenarios were considered when a solute atom replaces different sites in terms of their local Ti-Mo chemistry at the GB plane to calculate the distribution of segregation energies. The solute segregation to a Mo site at the GB plane is preferred rather than to a Ti site. Further analysis shows that these segregation energy trends can be rationalized based on a primarily elastic interaction. Thus the segregation energy scale with the solute size such that Y has the largest segregation energies followed by Zr and Nb.

Keywords: Solute segregation, Ti-Mo alloys, first-principles, grain boundary

I. INTRODUCTION

Titanium and its alloys are commercially important materials and have in particular applications in biomedical and aerospace industries [1]. While many allotropes of Titanium exists, there are three important ones: the α -phase (hcp) is stable at low temperature and atmospheric pressure, the β -phase (bcc) is stable at high temperature and atmospheric pressure and the ω -phase (hexagonal) is stable at high pressures [2]. Apart from temperature and pressure, various alloying elements are added in order to achieve stability of the different phases to arrive at a desirable microstructure including dual-phase α - β structures [3]. Solute elements may significantly affect the microstructure evolution and the mechanical properties of Ti alloys [4]. This is in part attributed to segregation to grain boundaries (GBs) and other interfaces. Recent advances in atomic-scale characterization using atom probe tomography have made it possible to study solute segregation at interfaces in many metallic alloy systems [5, 6]. On the other hand, atomistic simulations provide a detailed and efficient way to analyze the segregation behavior of various solute elements [7]. First-principles simulations in Ti have been limited to the α -phase mainly focusing on segregation of non-metallic interstitial elements and transition metals [8, 9] to twin and symmetric tilt GBs. First-principles studies of segregation in the β -phase are challenging because this phase is thermodynamically and mechanically unstable at 0 K.

There are three approaches to stabilize β -Ti using first-principles studies: one is to perform *ab initio* molecular dynamics (AIMD) at high-temperatures [10], second is alloying with a β -phase stabilizing element such as Mo and V [11] and third is to apply pressure to the system [12]. Due to the exorbitant computationally expensive nature of AIMD calculations and the un-physical nature of pressure for evaluating solute segregation, the alloying strategy in β -Ti is considered for predicting solute segregation to grain boundaries. Raabe *et al.* [13] showed that 25 at.% Mo is required to thermodynamically and mechanically stabilize the bcc phase over the hcp phase. Yan *et al.* [14] have also used alloying as a tool to investigate the segregation of Y and B in Ti-Mo and Ti-V alloys. They employed the virtual crystal approximation (VCA) method where each atomic site is a representative alloy with the overall composition. Their work shows that Y tends to segregate while B tends to de-segregate at the $\Sigma 3[110]/(111)$ GB.

Investigating defect structures and energetics in alloy systems using first-principles calculations has been a recent field of study. An emerging body of literature is available on evaluating point-defect energetics such as vacancy formation energies in binary and multi-component alloys [15–20] whereas similar simulations for planar defects in alloys are still in their evolving state. Shen *et al.* [21] have investigated the GB formation energies as a function of Mo and Nb alloying elements in bcc γ -U. Their work shows that $\Sigma 3[110]/(111)$ and $\Sigma 5[100]/(013)$ grain boundary structures are stable at greater than 27 at.% Mo and 30 at.% Nb. Scheiber *et al.* [22] studied Re segregation and work of separation for various $\langle 110 \rangle$ symmetric tilt grain boundaries in W-25 at.% Re alloys. Their studies show that segregation of Re increases the work of separation which is consistent

with experimental observations in W-Re alloys. These simulations were limited to a few configurations of the alloy structure and solute substitution in the host metal.

We study in this work the segregation of a solute species in a binary alloy. Using density functional theory (DFT) calculations, the binary Ti-25at.%Mo alloy is represented with the special quasi-random structure (SQS) approach and all possible configurations with the solute are included when evaluating the energetics of the bulk and GB structure. Representative values are computed and analyzed for bulk solution energies and segregation energies of Y, Zr and Nb to the $\Sigma 5(130)[001]$ GB in a Ti- 25 at.% Mo alloy. Further, segregation of the host elements (Ti and Mo) to the GB plane are calculated and finally the computed energies are analysed in terms of the local volume and chemistry.

II. COMPUTATIONAL METHOD

A. Structural models for bulk and GBs

Ti-25 at.% Mo is chosen as the alloy composition for our calculations. The random alloy is modelled within the SQS super-cell approach wherein the alloy constituents are distributed randomly within the cell. For creating the SQS alloy structures, the Warren-Cowley short range order (SROs) parameter [23, 24] is computed for six consecutive nearest neighbor (NN) shells to ensure low short range order within the simulation cells. A structure with SRO=0 for first NN and SRO < 0.01 for the other five shells is considered as a representative Ti-Mo alloy structure. For the bulk structure, a 128 atom supercell is used with dimensions of $12.85 \times 12.85 \times 12.85 \text{ \AA}^3$ as shown in Figure 1a. In order to obtain energies of a Ti and Mo atom in a Ti- 25at.% Mo structure, a 125 atom supercell is also created (which contains 93 Ti with 31Mo + 1Mo), i.e., with a slightly higher (25.6 at.%) Mo content. The SROs of the 125 atom supercell is set to be similar to that of the 128-atom supercell. For creating the GB structure, first a 60-atom bulk structure is generated with similar SROs as the 128-atom supercell with x, y, z axes aligned as [130], $[\bar{3}10]$ and [001] crystallographic directions respectively. A $\Sigma 5(130)[001]$ GB bcc Ti-25 at.% Mo structure with dimensions of $10.16 \times 20.32 \times 9.64 \text{ \AA}^3$, containing 120 atoms is constructed by choosing a y-plane to mirror across in 60 atom supercell. Ten different alloy GB structures are possible to create with this approach. Out of the ten, two GB structures are selected to study solute segregation. These structures are highlighted in Figure 1b and Figure 1c.

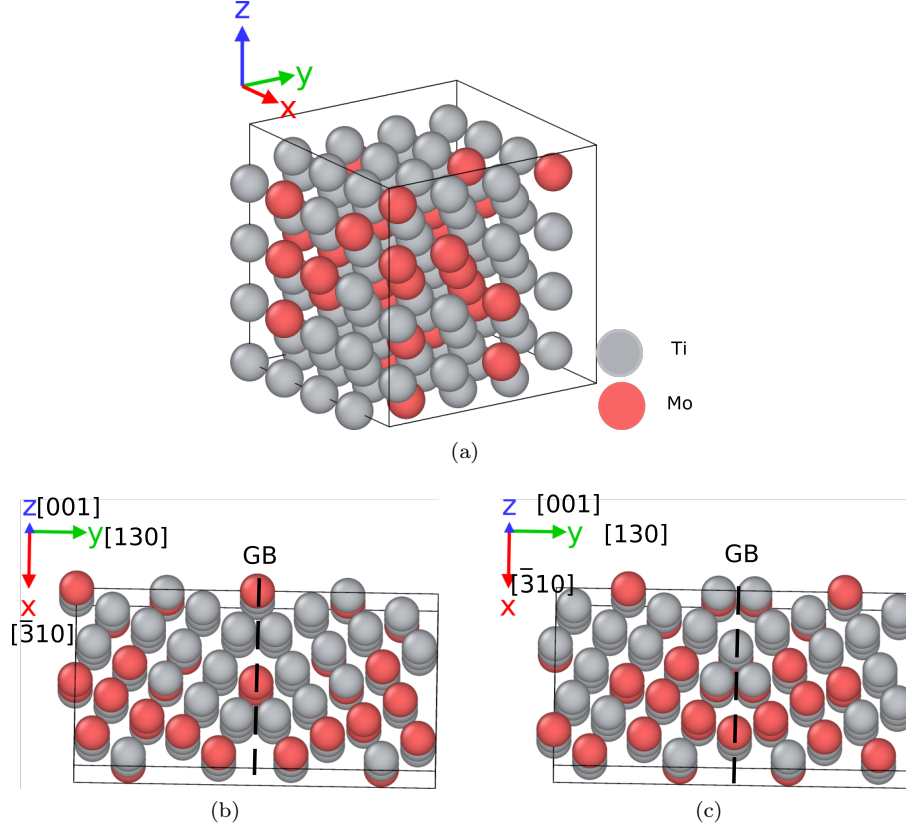


Figure 1: Schematic of all DFT supercells used in the study, grey and red atoms refer to Ti and Mo sites, respectively. (a) 4x4x4 bulk supercell of 128 atom alloy structure (b) GB-I and (c) GB-II alloy structure

B. First-principles calculations

DFT calculations are conducted using the Vienna *ab initio* simulation package (VASP) with the projector augmented wave (PAW) pseudopotentials [25, 26], and the Perdew-Burke-Ernzerhof (PBE) generalized gradient approximation (GGA) [27] for the exchange-correlation functional to arrive at the ground-state structures and energies. To truncate the plane-wave expansion, 360 eV energy cutoff is adopted. A k-mesh density of 0.02 \AA^{-1} is employed to sample the Brillouin zone. The outermost electron shell (and number of electrons) in the pseudo potentials used for Ti, Mo, Y, Zr and Nb are 4s (12), 5s (14), 5s (11), 5s (12), 5s (13), respectively. A force cutoff of 0.01 eV \AA^{-1} is adopted for the positions only relaxation step and an energy cutoff of 10^{-8} eV is used for the volume only relaxation step. Periodic boundary conditions without vacuum are adopted since otherwise the free surfaces cause instability in the simulations. The Birch-Murnaghan equation of state (EoS) method [28] is employed to relax the GB and GB-solute structures. It is often found that varying the supercell length perpendicular (i.e., y-direction as shown in Figure 1b) to the GB plane changes the excess volume of the GB, δV , and thus the GB energy [29]. In our study, the length of the supercell normal to the plane is varied in steps of 0.2 \AA to change the volume. Four such calculations are performed in order to obtain the minimum energy for each GB and this GB structure is then used for any further calculations. Finally, solute substitution is only done at the GB habit plane in order to preserve symmetry. For the post-processing step, modules from pymatgen [30] and pyiron [31] codebases are used to perform the EoS fits and obtain the relevant information for Voronoi volume and local chemistry at each site.

III. RESULTS

A. Solute substitution in bulk

The lattice constant of the Ti-25 at.% Mo alloy is found to be 3.213Å. All 128 sites in the alloy bulk structure are substituted by a third species, i.e., the solute. There are two host species (Ti and Mo) substitutions for the solute. Since each of the sites has a different local environment, there is a distribution in the solute solution energy. In order to compute bulk solution energies, we first calculate the energy of one Mo atom ($E_{\text{Mo,alloy}}$) and one Ti atom ($E_{\text{Ti,alloy}}$) in the Ti-25 at.% Mo alloy to obtain the chemical potential of the two species using:

$$E_{\text{Mo,alloy}} = [E_{125}(93, 32, 0) - \frac{31}{32} \cdot E_{128}(96, 32, 0)] \quad (1)$$

$$E_{\text{Ti,alloy}} = \frac{1}{3} \cdot [E_{128}(96, 32, 0) - E_{125}(93, 32, 0)] \quad (2)$$

In the above notation, the number of atoms of each species is given inside the parenthesis. The first number refers to the majority species, Ti, the next two numbers refers to the count of Mo atoms and the solute species, respectively. Bulk solution energy of solute X at a Ti site is defined as follows:

$$E_{\text{X@Ti}}^{\text{sol}} = E_{128}(95, 32, 1) - E_{128}(96, 32, 0) - E_{\text{X,ref}} + E_{\text{Ti,alloy}} \quad (3)$$

Similarly, for substitution of solute, X at a Mo site one has:

$$E_{\text{X@Mo}}^{\text{sol}} = E_{128}(96, 31, 1) - E_{128}(96, 32, 0) - E_{\text{X,ref}} + E_{\text{Mo,alloy}} \quad (4)$$

$E_{\text{X,ref}}$ refers to the energy of a single solute atom in their ground state structure. For Y and Zr, the hcp structure and for Nb, the bcc crystal structure is relaxed to obtain the respective per-atom solute reference energies.

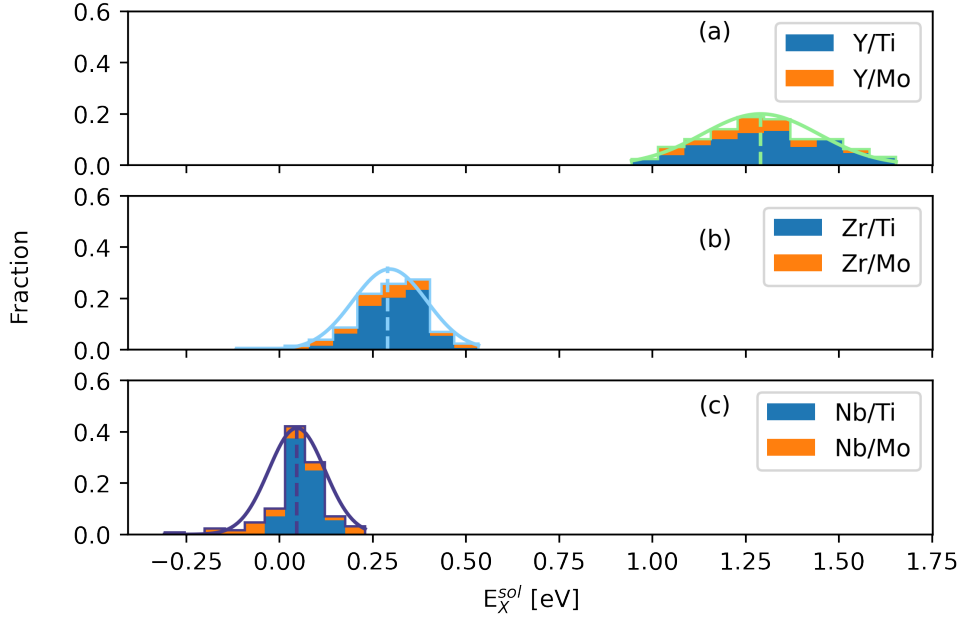


Figure 2: DFT calculated bulk solution energy distributions (out of 128 data points) of (a) Y, (b) Zr and (c) Nb in a Ti- 25at.% Mo alloy. Solution energy distributions of each solute is split into Ti and Mo site distributions indicated by blue and orange bars, respectively. The vertical dashed lines represent the mean value of the individual distributions.

The two distributions ($E_{X@Ti}^{sol}$ and $E_{X@Mo}^{sol}$) can be reconciled into a single distribution E_X^{sol} for each solute as shown in Figure 2 using the approach given by equation (3) and equation (4)). These distributions can be described with normal distributions characterized by a mean value and standard deviation. Please note, in the case of pure systems, these distributions collapse into a single value or a Dirac delta distribution. The atomic sites which are at the mean value are considered as “representative sites” for the solutes in the bulk. From Figure 2, we find that Y (mean: 1.29 eV, std: 0.16 eV) has a strong tendency to not dissolve in the bulk followed by Zr (mean: 0.3 eV, std: 0.1 eV). This can be rationalized based on the size of solute atoms, Y being a larger solute atom has the least tendency to dissolve in the bulk. The range for Y solution energies is 1.0 - 1.7 eV and for Zr, the range of solution energies is 0.1 - 0.5 eV. On the other hand, Nb, has comparatively minor solution energies with a mean of 0.03 eV and a standard deviation of 0.08 eV. Favourable dissolution, i.e. $E_{sol}^X < 0$ occurs for Nb when replacing Mo atoms in the original bulk alloy as illustrated in Figure 2 (c). Although there exists a single distribution, minor differences between the individual distributions for Ti and Mo host substitutions are found. For Y, Zr and Nb, the difference between $\langle E_{X@Ti}^{sol} \rangle - \langle E_{X@Mo}^{sol} \rangle$ are 45, 48 and 56 meV, respectively using the mean values of the distributions shown above. Representative bulk sites are identified when the solute substitutes at a Ti site and Mo site, respectively. The solution energies for these representative Ti and Mo sites ($E_{rep}(95, 32, 1)$ and $E_{rep}(96, 31, 1)$) are 1.33, 0.29, 0.04 eV and 1.28, 0.31, 0.03 eV for Y, Zr and Nb, respectively.

B. Grain boundary energy of different GB configurations

When creating the Ti-25 at.% Mo alloy GB structure, there are many possibilities on mirroring across the y-plane in the bulk supercell. This leads to different arrangements of Ti and Mo sites in the GB structure and as a result there are varying concentration of Mo at the GB. There are ten possible GBs in the present case but only five of them have stable configurations. The other five configurations contain less than 20 at.% Mo in either the bulk or the GB region of the supercell and lead to significant reconstruction.

In order to characterize the concentration of Mo at the GB, the structural unit model of a $\Sigma 5$ alloy GB is used, as highlighted in Figure 3. From the schematic, it is clear that the structural repeat units (5 atoms

for each unit in $\Sigma 5$) can have different arrangement of Mo atoms in them. To quantify the concentration of Mo in the GB region, the ratio of number of Mo (small-sized) atoms to the number of GB (shown in grey) atoms is used.

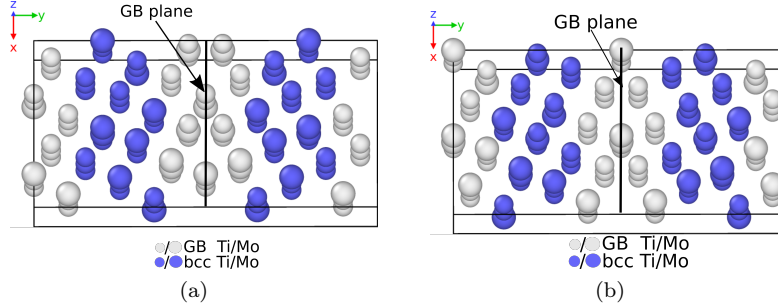


Figure 3: Schematic showing the structural units of $\Sigma 5(130)[001]$ GB-1 and GB-2 structure in (a) and (b), respectively. GB atoms are shown in grey and bulk bcc atoms in blue. Ti and Mo species are shown by small and large atoms, respectively.

The GB energy (γ_{GB}) is computed as follows:

$$\gamma_{GB} = [E_{GB}(90, 30, 0) - 90 \cdot E_{Ti, alloy} - 30 \cdot E_{Mo, alloy}] / (2 \cdot A_{GB}) \quad (5)$$

Here, A_{GB} refers to the area of the GB, and a factor of two is introduced to account for two GBs since periodic boundary conditions are used. $E_{GB}(90, 30, 0)$ refers to the energy of the Ti- 25at.% Mo GB supercell, which varies according to individual arrangements of Ti and Mo atoms in the GB structure. Table I summarizes the GB energy together with the chemical compositions of the GB unit cells as well as the GB planes.

Table I: GB energy-concentration data for five stable configurations

S.No	at.% Mo in GB unit cell (out of 60 atoms)	at.% Mo at GB plane (out of 12 atoms)	GB energy, γ_{GB} (mJ m ⁻²)
1	20	16.6	895
2 (GB-I)	23.3	33.3	1100
3 (GB-II)	23.3	50	994
4	26.7	33.3	1083
5	30	33.3	1011

As shown in Table I, the GB energies are found to be approximately 1 J m⁻², with a 10% variation from 0.9 J m⁻² to 1.1 J m⁻². Within this range of variation, there is no clear trend with the Mo content in the GB plane or GB unit cell. Nevertheless, the lowest GB energy is for the structure with the lowest Mo concentration at the GB unit cell and GB plane. Similarly, Shen *et al.* [21] predicted a non-linear variation of GB energy in bcc U as function of Mo or Nb content. Further, the role of domain size has been evaluated by conducting a simulation with a 240-atom cell for the GB-II configuration. In this case, the calculated GB energy is 966 mJ m⁻², i.e. within 30 mJ m⁻² of the GB energy of the 120 atom cell such that it is concluded that this smaller domain size is sufficient for convergence of the GB simulations.

C. GB Segregation in Ti-Mo alloy

1. Segregation energies of Ti/Mo to the GB plane

The two GBs with 23.3 at.% Mo in the GB unit cell which is close to the alloy composition are selected for solute substitution in the GB habit plane. Based on the local GB site chemistries, there are six different segregation sites for each species, i.e. 3 sites for Ti and Mo each at GB-I and 4 and 2 sites for Ti and Mo sites at GB-II, respectively. First, the segregation energies of Mo and Ti atoms in the binary Ti-Mo system to the GB plane are calculated as follows:

$$E_{\text{Mo@Ti}}^{\text{seg}} = [E_{\text{GB}}(89, 31, 0) - E_{\text{GB}}(90, 30, 0)] - [E_{\text{rep}}(95, 33, 0) - E_{128}(96, 32, 0)] \quad (6)$$

$$E_{\text{Ti@Mo}}^{\text{seg}} = [E_{\text{GB}}(91, 29, 0) - E_{\text{GB}}(90, 30, 0)] - [E_{\text{rep}}(97, 31, 0) - E_{128}(96, 32, 0)] \quad (7)$$

In order to calculate the two quantities above, we need a representative site for a Mo atom at a Ti site in the bulk alloy and similarly for a Ti atom at a Mo site. We take the average of 96 data points for Mo substitution to be $E_{\text{rep}}(95, 33, 0; \text{bulk})$ and the average of 32 data points for Mo substitution to be $E_{\text{rep}}(97, 31, 0; \text{bulk})$. For the GBs, all sites at the GB plane are substituted for Ti and Mo at Mo and Ti sites, respectively and the results are included in Figure 4. In terms of statistics, we have 7 sites from GB-I (3 sites) and GB-II (4 sites) available for Mo substitution. Similarly, we have 5 sites from GB-I (3 sites) and GB-II (2 sites) available for Ti substitution. Segregation energies of Ti have a mean of -0.33 eV and range from -0.44 to -0.23 eV. On the other hand, Mo segregation has a mean of 0.44 eV and a rather large range from 0.1 to 0.69 eV. These results indicate that Ti has a tendency to segregate to the GBs whereas Mo tends to de-segregate.

2. Solute segregation energies to the GB plane for GB-I and GB-II

The segregation energy of a solute, X to a Ti site is calculated as follows:

$$E_{\text{X@Ti}}^{\text{seg}} = [E_{\text{GB}}(89, 30, 1) - E_{\text{GB}}(90, 30, 0)] - [E_{\text{rep}}(95, 32, 1) - E_{128}(96, 32, 0)] \quad (8)$$

Similarly, for a Mo site, the segregation energy is computed as:

$$E_{\text{X@Mo}}^{\text{seg}} = [E_{\text{GB}}(90, 29, 1) - E_{\text{GB}}(90, 30, 0)] - [E_{\text{rep}}(96, 31, 1) - E_{128}(96, 32, 0)] \quad (9)$$

Figure 4 shows the segregation energies of the three solutes in GB-I and GB-II. For Y, there is a case when substituting Ti in GB-II leads to a structural change of the GB resulting in a large (-2.02 eV) segregation energy which is not shown in Figure 4. Overall, there is a clear trend for the segregation energies of the three solutes. Y has the strongest attraction to the GBs followed by Zr whereas Nb shows only comparatively weak attraction when replacing Mo but not when replacing Ti. This is consistent with their bulk misfit as shown above based on solution energies. Further, for all solutes replacing Mo in the GB is preferred as compared to Ti substitution which is consistent with the segregation energies of Mo and Ti at the GB sites in the binary Ti-Mo system, i.e. there is a preference of Ti segregation and de-segregation of Mo.

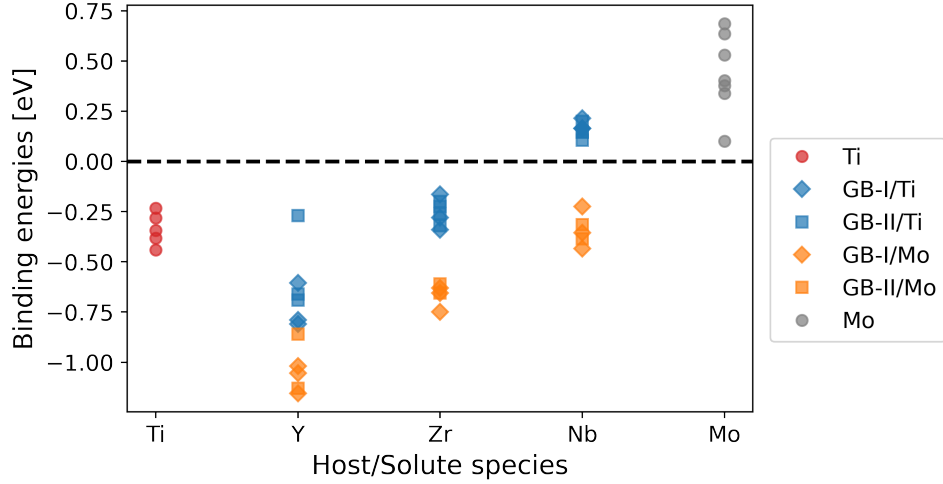


Figure 4: DFT computed segregation energies of Y, Zr and Nb to Ti and Mo host sites in GB-I (diamond markers) and GB-II (square markers). Individual points are colored based on whether Ti (blue) or Mo (orange) is substituted at the GB plane. Segregation energies below the dashed line suggest favorable segregation, while above the dashed line suggest unfavorable segregation.

IV. DISCUSSION

A. Bulk properties

In the bulk alloy, there are 128 sites of Ti and Mo in total. The Voronoi volume of these sites is shown in Figure 5 as a function of the number of Mo atoms in the first next neighbor (1nn) shell of each atomic site. With an increasing number of Mo atoms in the 1nn shell, the local Voronoi volume decreases for Ti and increases for Mo sites, respectively. On average, there is a linear trend in both cases. Further, the local volume of Ti sites is in general larger than that of Mo sites.

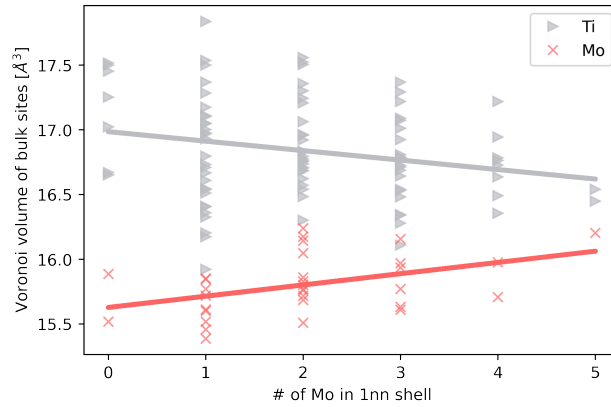


Figure 5: Voronoi volume of Ti and Mo sites in the bulk alloy as a function of number of Mo atoms in the 1nn shell (out of 8 atoms).

In order to decouple the local chemistry and local volume effects on the bulk solution energies, the trends between solution energies and Voronoi volume before solute substitution is investigated. As shown in Figure 6, the trends for Y, Zr and Nb's bulk solution energy are the same except for Nb on Ti sites where the solution energies are negligible. In general there is a linear decrease of solution energies with increasing site volume. This trend is particularly pronounced for Y when replacing Ti.

The negative slope can be rationalized by size effects, Y being a larger solute atom prefers to dissolve in sites which are larger in size in the distribution of available sites. Similarly, Zr has a moderate linear dependence with the Voronoi volume indicating the size effects persists although to a smaller extent than for Y. In the case of Nb, the dependence with the volume is negligible and this can be rationalised by the fact that Nb is a smaller solute compared to the other two solutes.

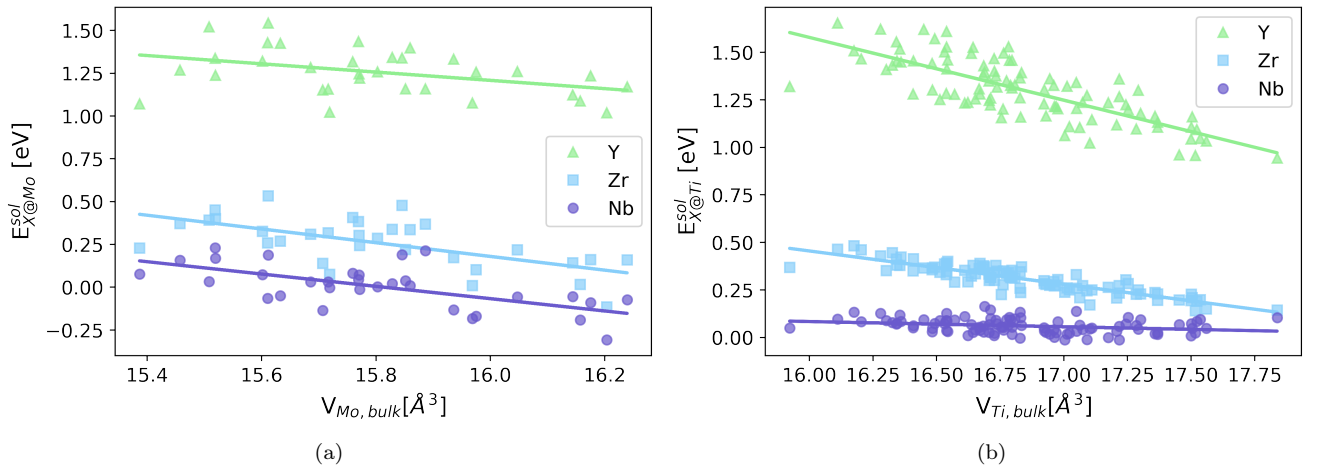


Figure 6: (a) Computed bulk solution energy at a Mo site plotted as a function of Voronoi volume of the same Mo site before solute substitution. (b) Computed bulk solution energy at a Ti site plotted as a function of Voronoi volume of the same Ti site before solute substitution

In addition to site volume, the local neighborhood can affect the bulk solution energy distribution. To analyze the potential chemistry effect the number of Mo/Ti atoms in the 1nn shell may be considered as a measure. The results of this analysis are shown in figure 7. As noted in ref. [15], the slopes of the trend lines are essentially the interaction parameters between the solute and the host atom that the solute is being substituted for. Slopes of the lines of Nb (-0.1 eV/at) and Zr (-0.09 eV/at) substituting a Mo site indicate towards to favourable dissolution when increasing the number of Mo atoms in the local chemical neighborhood. This could be because of chemical interaction (i.e., electronegativity) between Nb and Mo as found in [32] when studying high-entropy alloys containing Mo and Nb. Another key observation is the dissolution of Y in a Ti site (slope of -0.08 eV/at); it becomes favorable to dissolve a Y atom in a Ti site with local neighborhoods having a higher number of Ti atoms. This can be rationalized by the strain-relief argument where Y atom likes to dissolve at the larger volume (Ti) sites than smaller volume (Mo) sites as seen in figure 6(a) and figure 6(b), respectively. This variation indicates that there might be synergistic effects of local volume and chemistry for the case of Y at Ti substitution. Finally, there is almost no correlation between Nb and Zr substitution energies at Ti sites and the number of Ti in the first neighbor shell. This is true for Y substitution at Mo sites as well. Thus, the dominant effect on the bulk solution energies is the local Voronoi volume for these cases.

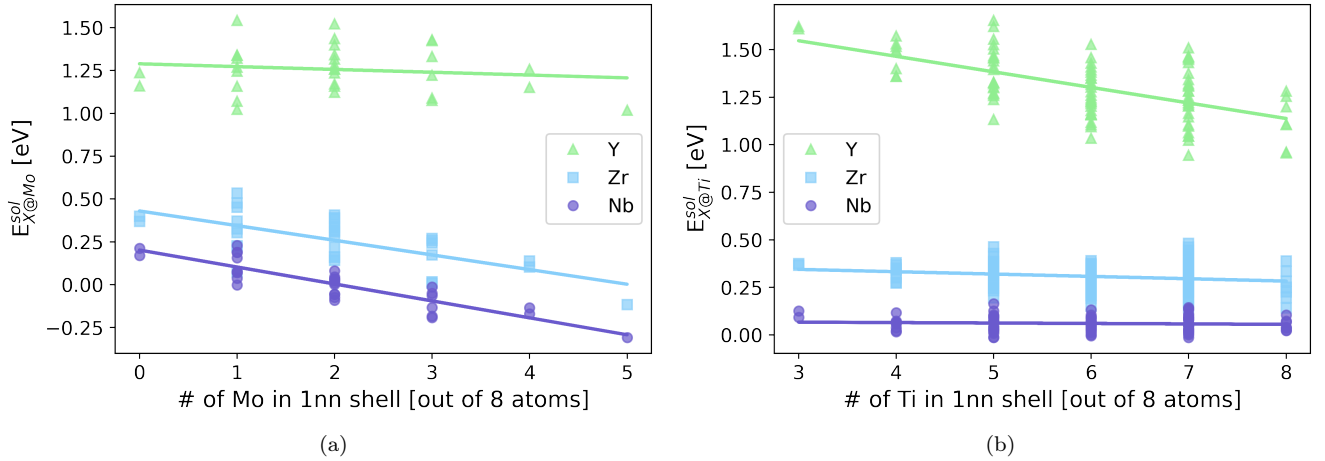


Figure 7: (a) Computed bulk solution energy at a Mo site plotted as a function of number of molybdenum atoms in first nearest neighbor (1nn) shell around each solute-substituted site. (b) Computed bulk solution energy at a Ti site plotted as a function of number of titanium atoms in first nearest neighbor (1nn) shell around each solute-substituted site. The trend lines are obtained by averaging the values at number of sites having the same # of Ti/Mo atoms in 1nn shell.

B. GB properties

The differences in solute segregation to Ti and Mo sites are analyzed in further detail. First, a discussion on Voronoi volume of the undecorated and decorated GB site is presented. A trend analysis of segregation energies with Voronoi volume of clean GB sites shows that the segregation energies of various solute-host pairs are essentially independent of the Voronoi volume of clean GB sites. Next, the trends of solute segregation energies as a function of Voronoi volume of solute substituted sites is presented as shown in Figure 8a where at least for Y the magnitude of the segregation energy increases with site volume. The trends for Zr and Nb remain negligible. Although the individual data for Ti and Mo substitution seem to have similar volume ranges, the segregation energies vary for both cases.

However, the volume difference before and after solute substitution provides a clearer trend for the resulting segregation energies. This is shown in figure 8b, where the x-axis represents the change in site volume between solute segregated site and that of the clean GB site, i.e. $\Delta V_{X \rightarrow Ti/Mo} = V_{X,i} - V_{Ti/Mo,i}$. Here, $V_{X,i}$ is the Voronoi volume of solute at GB site i and $V_{Ti/Mo,i}$ is the Voronoi volume of the Ti/Mo atom at the same GB site i . A general observation is that a volume increase favours segregation whereas a decrease in volume leads to a positive, i.e. unfavourable, segregation energy as is the case for Nb on Ti sites. Nb segregating to a Ti site occupies a smaller volume than its undecorated counterpart site which is associated with positive (unfavourable) segregation energies. Further, a general trend is that the volume changes for Mo sites are larger than for Ti sites and hence this further indicates why the magnitude of favourable segregation energies to a Mo site is larger. This volume difference scales linearly with the solute segregation energy, where a larger volume difference implies a stronger solute segregation.

A consistent shift of segregation energies when replacing Mo versus Ti is also predicted for Y, Zr and Nb, i.e. the attraction for these solutes to the GB is larger when replacing Mo. Excluding the outlier (-0.25 eV) for Y at Ti host substitution, differences between $\langle E_{X@Ti}^{bind} \rangle$ and $\langle E_{X@Mo}^{bind} \rangle$ for Y, Zr and Nb are 0.41, 0.41 and 0.50 eV, respectively. However, these differences do not exactly match with the difference of 0.77 eV between Ti and Mo segregation energies in the Ti-Mo system (see Figure 4). Thus, there is also a solute specific role in changing the GB site volume.

The above analysis indicates that elastic interactions are significant for the magnitude of the segregation energies. In order to obtain average segregation energies, the evaluation of an Eshelby-type approach may be considered using information of the undecorated GB structures as proposed in previous studies [33, 34].

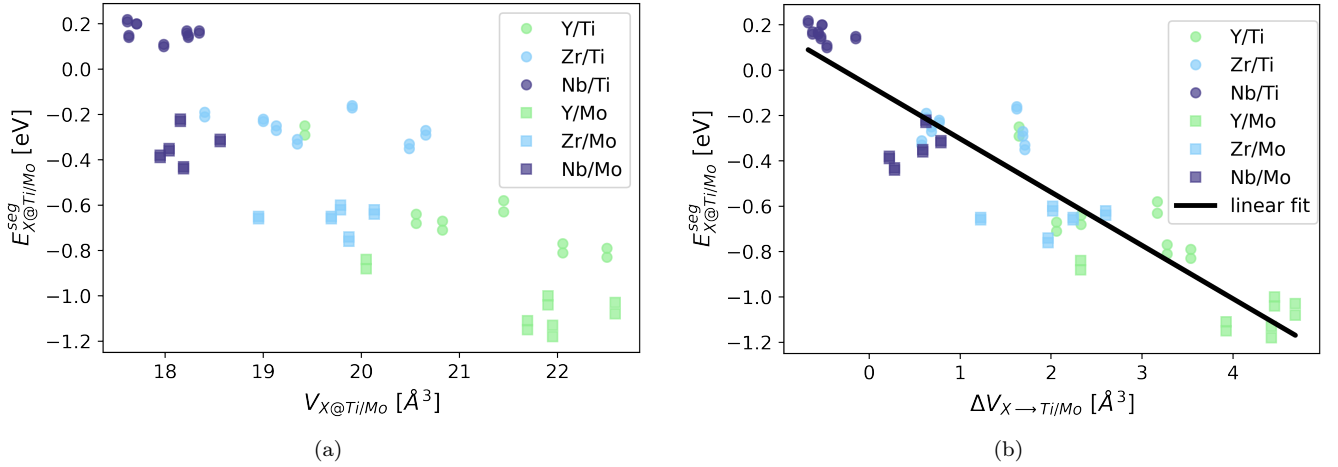


Figure 8: (a) DFT computed segregation energies of Y, Zr and Nb to Ti (circles) and Mo (squares) host sites in GB-I and GB-II as a function of Voronoi volume of solute substituted sites ($V_{X@Ti/Mo}$) (b) DFT computed segregation energies of Y, Zr and Nb to Ti (circles) and Mo (squares) host sites in GB-I and GB-II as a function of volume difference between Voronoi volume after and before solute substitutions at GB plane sites ($\Delta V_{X \rightarrow Ti/Mo}$)

From Figure 8b, it is seen that there is primarily elastic contribution to the segregation energies of solutes. Scheiber *et al.* [35] have proposed an expression which captures these interactions based on an Eshelby-type model [36, 37] :

$$E_{X@Ti/Mo}^{seg,el} = \frac{-(V_A - V_B)^2}{\left(\frac{3}{2} \cdot \frac{V_A}{G_A} + 2 \cdot \frac{V_B}{K_B}\right)} + \frac{(V_A^{GB} - V_B)^2}{\left(\frac{3}{2} \cdot \frac{V_A^{GB}}{G_A} + 2 \cdot \frac{V_B}{K_B}\right)} + \frac{-(V_A^{GB} - V_A)^2}{\left(\frac{3}{2} \cdot \frac{V_A^{GB}}{G_A} + 2 \cdot \frac{V_A}{K_A}\right)} \quad (10)$$

Here, V_A , V_B and V_A^{GB} refers to bulk volume of host and solute as well as volume of the GB sites, respectively. The elastic properties, G_A , K_A and K_B are shear modulus of host, bulk modulus of host and solute, respectively. These properties for the host atom are taken to be that of Ti-Mo alloys: 100 GPa for Young's modulus from [14] and a poisson's ratio of 0.33 was assumed which allowed to calculate G_A and K_A to be 98 GPa and 37.6 GPa, respectively. V_A is determined based on the calculated lattice constant for the Ti-Mo alloy of 3.213 \AA . In the case of Y, Zr and Nb as solutes (B), the properties are taken from Bakker [38]. As proposed by Scheiber *et al.* a scaling constant c can be introduced for V_A^{GB} to improve fits to the calculated segregation energies by changing the clean GB site volume by multiplying it with c . Since, there exists a difference in solute segregation energies when substituting Ti or Mo sites (see Figure 4), two scaling factors (c_{Ti} and c_{Mo}) are quantified, one for each host species. The scaling factors c_{Ti} and c_{Mo} , are found to be 1.2 and 1.5, respectively reflecting the larger volume change of Mo sites after solute substitution. Whilst, these models do not capture the true complexity of each site they still give overall trends of solute segregation energy predictions for the considered alloy system. The predictions from the model based on elastic interactions are summarized in Figure 9 indicating that the Y and Zr average segregation energies can be explained well within this framework, while Nb predictions are a bit off in from the DFT calculated values. Thus, other factors as e.g. chemical interactions may affect the segregation energies of smaller-sized solutes such as Nb. Still, the deviations are within 0.25 eV and general trends among the solutes are predicted correctly, nonetheless. If reasonable predictions could be made in this way one would not have the need for performing various solute-GB calculations. For example, it was observed by Huber *et al.* [33] that solute segregation energies of Pb and Mg in Al scale linearly with Voronoi volume of clean sites in symmetric and general tilt boundaries.

Using the above developed Eshelby-type model for two host sites- Ti and Mo, average GB solute segregation energies for other transition metal (TM) solutes can be estimated for the Ti- 25 at%. Mo alloy. In Figure 10

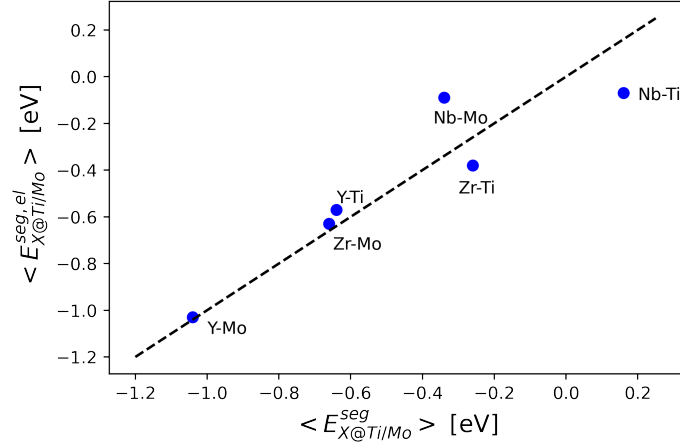


Figure 9: Comparison of average of segregation energies for Y, Zr and Nb to Ti and Mo sites calculated using DFT and Eshelby-type model

(a), the predicted energies are presented using the scaling constants obtained above for Ti and Mo sites, as well as the data for bulk modulus and volume of solutes from Bakker [38]. The observed trends correlate strongly with the solute volume shown in Figure 10(b). The larger solutes show similar behaviour as Y and Zr, i.e. they have a tendency to segregate to the GB with a preference for the Mo sites. On the other hand, smaller solutes, i.e. those in the middle of the TM series, have a tendency to de-segregate and the repulsion from the Mo sites is larger than that from the Ti sites. Overall, the simplified analysis provides a first guidance regarding the solute-GB interaction for the given alloy provided elastic contributions are dominant.

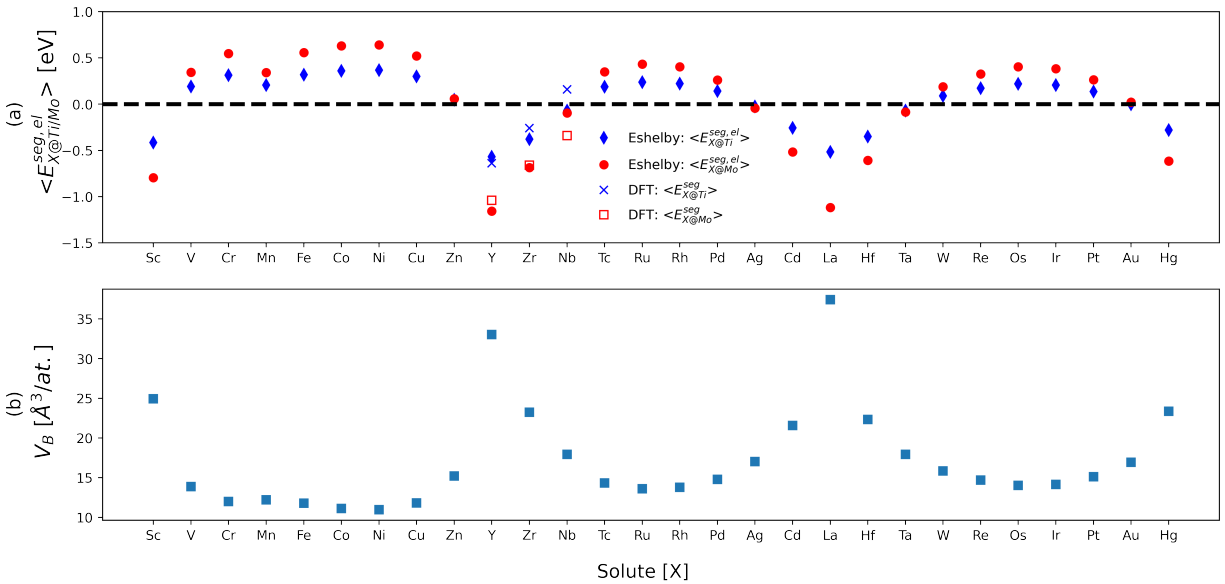


Figure 10: (a) Eshelby-type model predictions for segregation energies of (*3d*-, *4d*-, *5d*-) transition metal solutes to the $\Sigma 5$ GB plane in a Ti-Mo alloy system and average segregation energies of Y, Zr and Nb from DFT (b) Atomic volume of solute elements as taken from Bakker [38]

V. CONCLUSIONS

This study lays out a first-principles approach for investigating solute segregation in highly alloyed systems i.e., here Ti-25 at.% Mo based on the SQS approach. The main findings of this work are as follows:

1. A rigorous approach has been applied to determine solution energies in the bulk by considering all possible permutations in the simulation domain. The resulting solution energy distributions provide the basis to identify representative bulk energies for each considered solute. In the present case, i.e. for Y, Zr and Nb, elastic interactions dominate such that the volume of the bulk site rather than its local chemistry determine the mean solution energy which increase with solute size, i.e. $\text{Nb} < \text{Zr} < \text{Y}$. In these elastically dominated cases, the identification of the averaged bulk volume site in the alloy without solutes can be used to calculate the representative solution energy.
2. The solute segregation energies to GBs is also dominated by elastic interactions. The situation at the GB is, however, more complicated as the elastic interaction may be affected by the local chemistry. In the investigated cases, the change in GB volume sites before and after solute substitution has been identified as the critical aspect that determines the solute segregation energy. This volume change has been found to depend on which of the host species is replaced, i.e. it is larger for Mo sites than for Ti sites. Thus, the magnitude of segregation energies are larger when Mo sites are replaced and overall the segregation energies follow the solute size with Y having the largest attraction to the GBs followed by Zr and Nb.
3. Using an Eshelby-type approach with a host species dependent scaling factor for the grain boundary site volume provides a satisfactory description of the mean segregation energies computed from the DFT simulations for strongly segregating solutes (here Y, Zr), i.e. solutes that are significantly larger than the host atoms. The Eshelby-type analysis has been extended to three different series of transition metals showing a clear trend of segregation energies with solute size, i.e. larger solutes are more attracted to smaller host sites (Mo) and smaller solutes are less repelled from larger host sites (Ti).

ACKNOWLEDGEMENTS

The authors gratefully acknowledge the financial support under the scope of the COMET program within the K2 Center "Integrated Computational Material, Process and Product Engineering (IC-MPPE)" (Project No 886385). This program is supported by the Austrian Federal Ministries for Climate Action, Environment, Energy, Mobility, Innovation and Technology (BMK) and for Labour and Economy (BMAW), represented by the Austrian Research Promotion Agency (FFG), and the federal states of Styria, Upper Austria and Tyrol. This research was funded also in part by the Austrian Science Fund (FWF) (P 34179-N).

-
- [1] D. Banerjee, J. C. Williams, Perspectives on Titanium Science and Technology, *Acta Mater.* 61 (3) (2013) 844–879. doi:10.1016/j.actamat.2012.10.043.
 - [2] J. Zhang, Y. Zhao, R. S. Hixson, G. T. Gray, L. Wang, W. Utsumi, S. Hiroyuki, H. Takanori, Experimental constraints on the phase diagram of titanium metal, *J. Phys. Chem. Solids* 69 (10) (2008) 2559–2563. doi:10.1016/j.jpcs.2008.05.016.
 - [3] Y. Okazaki, Y. Ito, A. Ito, T. Tateishi, Effect of Alloying Elements on Mechanical Properties of Titanium Alloys for Medical Implants, *Mater. Trans., JIM* 34 (12) (1993) 1217–1222. doi:10.2320/matertrans1989.34.1217.
 - [4] M. Niinomi, Mechanical properties of biomedical titanium alloys, *Mater. Sci. Eng., A* 243 (1) (1998) 231–236. doi:10.1016/S0921-5093(97)00806-X.
 - [5] A. S. Ebner, S. Jakob, H. Clemens, R. Pippan, V. Maier-Kiener, S. He, W. Ecker, D. Scheiber, V. I. Razumovskiy, Grain boundary segregation in Ni-base alloys: A combined atom probe tomography and first principles study, *Acta Mater.* 221 (2021) 117354. doi:10.1016/j.actamat.2021.117354.
 - [6] B. Gault, A. Chiaramonti, O. Cojocaru-Mirédin, P. Stender, R. Dubosq, C. Freysoldt, S. K. Makineni, T. Li, M. Moody, J. M. Cairney, Atom probe tomography, *Nat. Rev. Methods Primers* 1 (51) (2021) 1–30. doi:10.1038/s43586-021-00047-w.

- [7] Y. Mishin, M. Asta, J. Li, Atomistic modeling of interfaces and their impact on microstructure and properties, *Acta Mater.* 58 (4) (2010) 1117–1151. doi:10.1016/j.actamat.2009.10.049.
- [8] D. A. Aksyonov, A. G. Lipnitskii, Solubility and grain boundary segregation of iron in hcp titanium: A computational study, *Comput. Mater. Sci.* 137 (2017) 266–272. doi:10.1016/j.commatsci.2017.05.034.
- [9] J. Hui, X. Zhang, T. Liu, W. Liu, B. Wang, First-principles calculation of twin boundary energy and strength/embrittlement in hexagonal close-packed titanium, *Mater. Des.* 213 (2022) 110331. doi:10.1016/j.matdes.2021.110331.
- [10] D. Korbmayer, A. Glensk, A. I. Duff, M. W. Finnis, B. Grabowski, J. Neugebauer, Ab initio based method to study structural phase transitions in dynamically unstable crystals, with new insights on the β to ω transformation in titanium, *Phys. Rev. B* 100 (10) (2019) 104110. doi:10.1103/PhysRevB.100.104110.
- [11] C. Marker, S.-L. Shang, J.-C. Zhao, Z.-K. Liu, Effects of alloying elements on the elastic properties of bcc Ti-X alloys from first-principles calculations, *Comput. Mater. Sci.* 142 (2018) 215–226. doi:10.1016/j.commatsci.2017.10.016.
- [12] Q.-M. Hu, S. Lu, R. Yang, Elastic stability of β -Ti under pressure calculated using a first-principles plane-wave pseudopotential method, *Phys. Rev. B* 78 (5) (2008) 052102. doi:10.1103/PhysRevB.78.052102.
- [13] D. Raabe, B. Sander, M. Friák, D. Ma, J. Neugebauer, Theory-guided bottom-up design of β -titanium alloys as biomaterials based on first principles calculations: Theory and experiments, *Acta Mater.* 55 (13) (2007) 4475–4487. doi:10.1016/j.actamat.2007.04.024.
- [14] J.-Y. Yan, H. Ehteshami, P. A. Korzhavyi, A. Borgenstam, $\Sigma 3(111)$ grain boundary of body-centered cubic Ti-Mo and Ti-V alloys: First-principles and model calculations, *Phys. Rev. Mater.* 1 (2) (2017) 023602. doi:10.1103/PhysRevMaterials.1.023602.
- [15] A. V. Ruban, Thermal vacancies in random alloys in the single-site mean-field approximation, *Phys. Rev. B* 93 (13) (2016) 134115. doi:10.1103/PhysRevB.93.134115.
- [16] H. B. Luo, Q. M. Hu, J. Du, A. R. Yan, J. P. Liu, Thermal vacancy formation enthalpy of random solid solutions: The FePt case, *Comput. Mater. Sci.* 143 (2018) 206–211. doi:10.1016/j.commatsci.2017.11.009.
- [17] A. Esfandiarpour, M. N. Nasrabadi, Vacancy formation energy in CuNiCo equimolar alloy and CuNiCoFe high entropy alloy: ab initio based study, *Calphad* 66 (2019) 101634. doi:10.1016/j.calphad.2019.101634.
- [18] Y. Zhang, A. Manzoor, C. Jiang, D. Aidhy, D. Schwen, A statistical approach for atomistic calculations of vacancy formation energy and chemical potentials in concentrated solid-solution alloys, *Comput. Mater. Sci.* 190 (2021) 110308. doi:10.1016/j.commatsci.2021.110308.
- [19] X. Zhang, S. V. Divinski, B. Grabowski, Ab initio prediction of vacancy energetics in HCP Al-Hf-Sc-Ti-Zr high entropy alloys and the subsystems, *Acta Mater.* 227 (2022) 117677. doi:10.1016/j.actamat.2022.117677.
- [20] X. Zhou, S. He, J. Marian, Vacancy Energetics and Diffusivities in the Equiatomic Multielement Nb-Mo-Ta-W Alloy, *Materials* 15 (15) (2022) 5468. doi:10.3390/ma15155468.
- [21] Z. Shen, Y. Kong, Y. Du, S. Zhang, Effect of alloying on stability of grain boundary in γ phase of the U-Mo and U-Nb systems, *Calphad* 72 (2021) 102241. doi:10.1016/j.calphad.2020.102241.
- [22] D. Scheiber, V. I. Razumovskiy, P. Puschnig, R. Pippan, L. Romaner, Ab initio description of segregation and cohesion of grain boundaries in W-25at.% Re alloys, *Acta Mater.* 88 (2015) 180–189. doi:10.1016/j.actamat.2014.12.053.
- [23] J. M. Cowley, An Approximate Theory of Order in Alloys, *Phys. Rev.* 77 (5) (1950) 669–675. doi:10.1103/PhysRev.77.669.
- [24] J. M. Cowley, Short-Range Order and Long-Range Order Parameters, *Phys. Rev.* 138 (5A) (1965) A1384–A1389. doi:10.1103/PhysRev.138.A1384.
- [25] P. E. Blöchl, Projector augmented-wave method, *Phys. Rev. B* 50 (24) (1994) 17953–17979. doi:10.1103/PhysRevB.50.17953.
- [26] G. Kresse, D. Joubert, From ultrasoft pseudopotentials to the projector augmented-wave method, *Phys. Rev. B* 59 (3) (1999) 1758–1775. doi:10.1103/PhysRevB.59.1758.
- [27] J. P. Perdew, K. Burke, M. Ernzerhof, Generalized Gradient Approximation Made Simple, *Phys. Rev. Lett.* 77 (18) (1996) 3865–3868. doi:10.1103/PhysRevLett.77.3865.
- [28] F. Birch, Finite Elastic Strain of Cubic Crystals, *Phys. Rev.* 71 (11) (1947) 809–824. doi:10.1103/PhysRev.71.809.
- [29] D. Scheiber, R. Pippan, P. Puschnig, L. Romaner, Ab initio calculations of grain boundaries in bcc metals, *Model. Simul. Mater. Sci. Eng.* 24 (3) (2016) 035013. doi:10.1088/0965-0393/24/3/035013.
- [30] S. P. Ong, W. D. Richards, A. Jain, G. Hautier, M. Kocher, S. Cholia, D. Gunter, V. L. Chevrier, K. A. Persson, G. Ceder, Python Materials Genomics (pymatgen): A robust, open-source python library for materials analysis, *Comput. Mater. Sci.* 68 (2013) 314–319. doi:10.1016/j.commatsci.2012.10.028.
- [31] J. Janssen, S. Surendralal, Y. Lysogorskiy, M. Todorova, T. Hickel, R. Drautz, J. Neugebauer, pyiron: An integrated development environment for computational materials science, *Computational Materials Science* 163 (2019) 24 – 36. doi:https://doi.org/10.1016/j.commatsci.2018.07.043.
URL <http://www.sciencedirect.com/science/article/pii/S0927025618304786>
- [32] D. F. Rojas, H. Li, O. K. Orhan, C. Shao, J. D. Hogan, M. Ponga, Mechanical and microstructural properties of

- a CoCrFe_{0.75}NiMo_{0.3}Nb_{0.125} high-entropy alloy additively manufactured via cold-spray, *J. Alloys Compd.* 893 (2022) 162309. doi:10.1016/j.jallcom.2021.162309.
- [33] L. Huber, B. Grabowski, M. Militzer, J. Neugebauer, J. Rottler, Ab initio modelling of solute segregation energies to a general grain boundary, *Acta Mater.* 132 (2017) 138–148. doi:10.1016/j.actamat.2017.04.024.
- [34] W. T. Geng, A. J. Freeman, G. B. Olson, Influence of alloying additions on grain boundary cohesion of transition metals: First-principles determination and its phenomenological extension, *Phys. Rev. B* 63 (16) (2001) 165415. doi:10.1103/PhysRevB.63.165415.
- [35] D. Scheiber, R. Pippan, P. Puschnig, A. Ruban, L. Romaner, Ab-initio search for cohesion-enhancing solute elements at grain boundaries in molybdenum and tungsten, *Int. J. Refract. Met. Hard Mater.* 60 (2016) 75–81. doi:10.1016/j.ijrmhm.2016.07.003.
- [36] J. D. Eshelby, *The Continuum Theory of Lattice Defects*, in: *Solid State Physics*, Vol. 3, Academic Press, Cambridge, MA, USA, 1956, pp. 79–144. doi:10.1016/S0081-1947(08)60132-0.
- [37] J. D. Eshelby, Distortion of a Crystal by Point Imperfections, *J. Appl. Phys.* 25 (2) (1954) 255–261. doi:10.1063/1.1721615.
- [38] H. Bakker, *Enthalpies in Alloys: Miedema’s Semi-empirical Model*, Trans Tech Publications, 1998.